2023 IEEE Symposium on Electromagnetic Compatibility & Signal/Power Integrity (EMC+SIPI) | 979-8-3503-0976-8/23/$31.00 ©2023 IEEE | DOI: 10.1109/EMCSIPI50001.2023.10241444

A Real-time Microwave Camera Prototype with Zero-bias Diode Detectors for EMI Source Imaging

Xin Yan*1, Liang Liu*2, and Victor Khilkevich*3
*EMC Laboratory
Missouri University of Science and Technology
Rolla, MO, USA
3khilkevichv@mst.edu

***Abstract*—Emission source microscopy (ESM) could be utilized to localize the Electromagnetic Interference (EMI) sources that contribute to the far-field radiation. In those cases, the electrical field over a two-dimensional plane is collected by mechanical scanning, resulting in a long measurement time and the presence of mechanical errors. In this work, a microwave camera based on a two-dimensional array of elliptical slot antennas and diode detectors is presented. Multiplexers are utilized to access the output of each detector and the scanning of the whole array could be done multiple times per second.**

Keywords—Emission source microscopy, microwave camera, diode detector

I. Introduction

As data rates and clock frequencies continue to increase, the EMI problems at several or tens of GHz have become more serious. Emission source microscopy (ESM) is a measurement method that can identify the radiating sources of a complex system. The complex field on a 2-D plane above the device under test (DUT) is measured and backpropagated to the source plane. In previous work on the ESM technique [1][2], dense and uniformly-distributed sampling points are picked on the scan plane, proving the best quality but leading to long measurement time. In [3], a sparse and nonuniform sampling method is applied to the ESM technique. It is proven that increasing number of samples proportionally increases the signal to noise (SNR) of reconstructed image for an ideal point source. The sparse ESM allows to select the number of samples based on the desired image quality, however, the human intervention is still needed. [4] presented an automatic method to select the sampling points based on the Gaussian process regression (GPR), which will predict the field distribution based on sparsely measured samples and select the next scanning location. The automatic GPR ESM method could further reduce the number of measurement points with less image quality degradation. The study in [5] shows how image quality is affected by numerical properties of the sparse ESM method.

However, although the sparse ESM method can greatly reduce the scanning time, the mechanical scanning system is still required, and the mechanical errors are always present [6]. Moreover, the scanning time is still the biggest obstacle limiting the efficiency of studying and mitigating the EMI in complex systems [7]. A real time imaging system may address the limitations of the traditional ESM methods in certain applications. A microwave camera built upon a two-dimensional array of switchable slot antennas was presented in [8]. In that design PIN diodes are utilized to engage the resonant elliptical slot antennas in the imaging system. The magnitude and phase

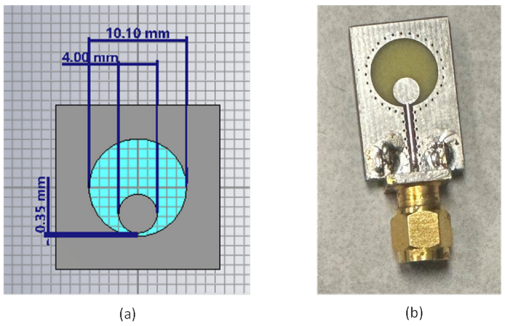

Fig. 1. (a) Antenna model. (b) Manufactured antenna prototype.

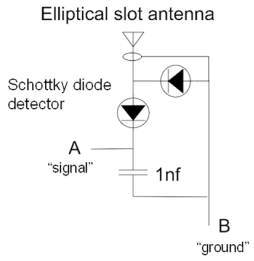

Fig. 2. Schematic of the diode detector.

of the antenna signals are measured, and the image is reconstructed based on the Synthetic Aperture Radar (SAR) technology. While providing an excellent image quality in real time, the system presented in [8] is complex and expensive.

In this paper, we propose an inexpensive design of a real-time microwave camera for EMI source imaging. A prototype 8 x 8 sensor array working up to 12 GHz is designed and presented. The antenna elements similar to those in [8] are used, but with integrated zero-bias diode detectors. Because of this no RF switching is required, and low frequency multiplexers are utilized to switch the detector outputs, thus reducing the complexity and cost of the array. Arduino Mega 2560 controller is utilized to control the multiplexer and measure the output of the diode detectors. Since only the magnitude of the signals is measured, an additional focusing system is required. A Fresnel zone plate is used for that purpose. The scanning of the whole array could be done multiple times per second, which is significantly faster compared to mechanical scanning. In the future work, a larger array will be designed and utilized to practical applications.

The paper is organized as follows. In Section II, the design of the proposed real time camera is introduced. Section III

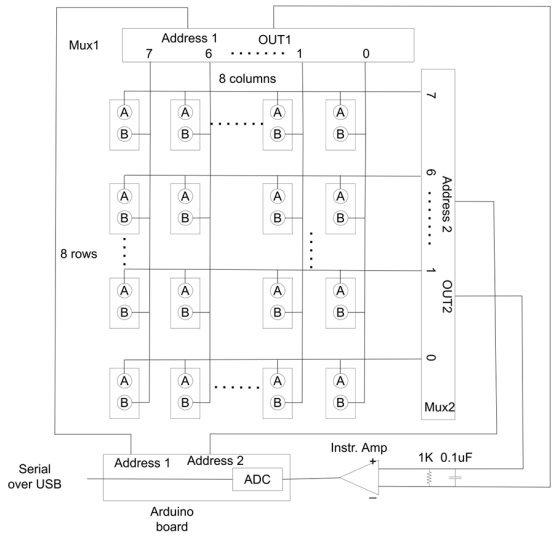

Fig. 3. Diagram of the camera sensor.

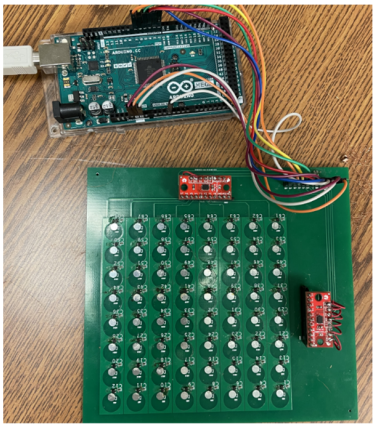

Fig. 4. The manufactured real time camera sensor.

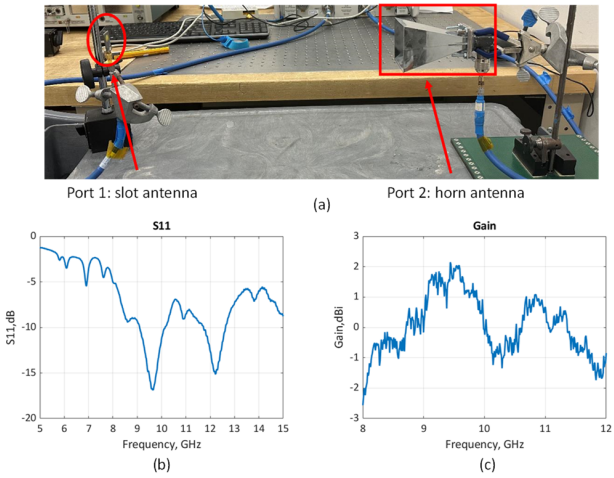

Fig. 5. Characterization of the elliptical slot antenna. (a) Measurement setup. (b) Reflection coefficient of the antenna. (c) Gain of the antenna.

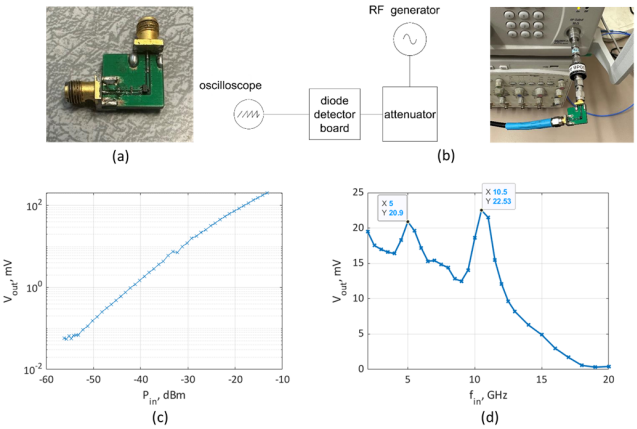

Fig. 6. Characterization of the detector board. (a) Photo of the board. (b) Measurement setup. (c) Sensitivity at 10 GHz. (d) Frequency response.

presents the characteristics of the camera and the measurement results. Section IV presents the conclusion.

II. Real-time Microwave Camera Design

The proposed prototype camera consists of 8 x 8 elliptical slot antenna elements with integrated zero-bias diode detectors. The target frequency band of the antenna elements is approximately 8-15 GHz. The model of the antenna is shown in Fig. 1 (a) and the dedicated prototype – in Fig. 1 (b).

The detector circuit diagram is shown in Fig. 2. A pair of the Schottky diodes (Infineon BAT15-04W [9]) and the 1 nF capacitor are added to each antenna element to produce a low frequency signal related to the RF amplitude. The diagram of the entire system is shown in Fig. 3. An Arduino Mega 2560 controller is utilized to switch the multiplexers and measure the output from each element. Two 8-to-1 multiplexers are used to select rows and columns respectively. The instrumentation amplifier is used to increase the sensitivity of the system. A shunt 1 kOhm resistor at the input of the amplifier is the load for the detectors and, and a shunt 0.1 uF capacitor provides additional filtering. It is worth noting that the off resistance of the multiplexer needs to be much higher than the detector load resistor in order to ensure DC decoupling between the array elements.

The proposed camera sensor is fabricated on a standard 2 layers PCB, as shown in Fig. 4. The thickness is 1.6 mm, and the dielectric is FR4. The slot antenna and the components are built on the top layer, the signal lines "A" are routed on the bottom layer, and the ground lines "B" – on the top one.

III. Characteristics of the Real Time Camera

A. Antenna and Detector Characterization

the dedicated slot antenna is characterized, as shown in Fig. 5. The reflection coefficient of the slot antenna is measured by a VNA. For the gain measurement the transmission coefficient between the elliptical slot antenna and a horn antenna with known gain is measured. The gain of the antenna is derived from Friis transmission equation:

$$G_{slot} = |S_{21}|^2 \frac{1}{G_{horn}} \left(\frac{4\pi d}{\lambda}\right)^2 \quad (1)$$

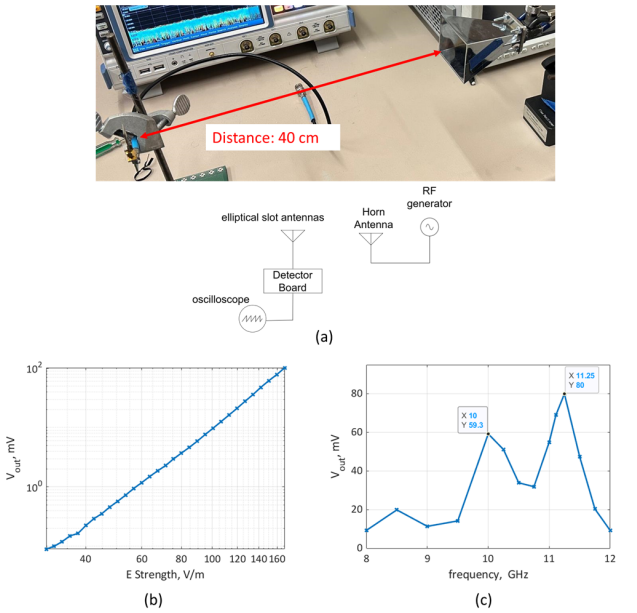

Fig. 7. Characterization of the single array element. (a) Measurement setup. (b) Sensitivity of the element. (c) Frequency response of the element.

where S_{21} is the transmission coefficient from the horn antenna to the slot antenna, G_{horn} is the gain of the horn antenna, and d is the distance between two antennas. The measured gain of the slot antenna in the X-band is between -2 and 2 dBi as can be seen from Fig. 5 (c).

A separate detector board is built, as shown in Fig. 6 (a). The 1 kOhm shunt resistor is added to the detector to get similar output as in the array element. To measure the sensitivity, as shown in Fig. 6 (b), the detector board is excited by a signal generator, and the output is measured using an oscilloscope. By decreasing the excitation amplitude, the minimum detectable power could be evaluated. As shown in Fig. 6 (c), the sensitivity of the detector circuit is about -53 dBm, corresponding to the output voltage just below 0.1 mV. Below that level the sensitivity was limited by the noise of the measurement instrument. By changing the frequency of the input signal, the frequency response of the detector board was also investigated. The results are shown in Fig. 6 (d). The input power is fixed at -35 dBm, and the frequency is swept from 2 GHz to 20GHz, with a 0.5 GHz step. As can be seen, the output voltage of the detector is relatively high below 12 GHz (the maximum operational frequency of the diodes according to the datasheet), with a peak level around 10.5 GHz.

Afterwards, the slot antenna is connected to the detector and the properties of the single array element is evaluated. The horn antenna connected to a signal generator is used as the signal source, as shown in Fig. 7 (a), and the output of the detector is measured by an oscilloscope. The distance between the horn antenna and the slot antenna is about 40 cm, and the E-field at the receiving antenna location is calculated as [10]:

$$E = \frac{\sqrt{30 \cdot P_{antenna} \cdot G_{horn}}}{d} \qquad (2)$$

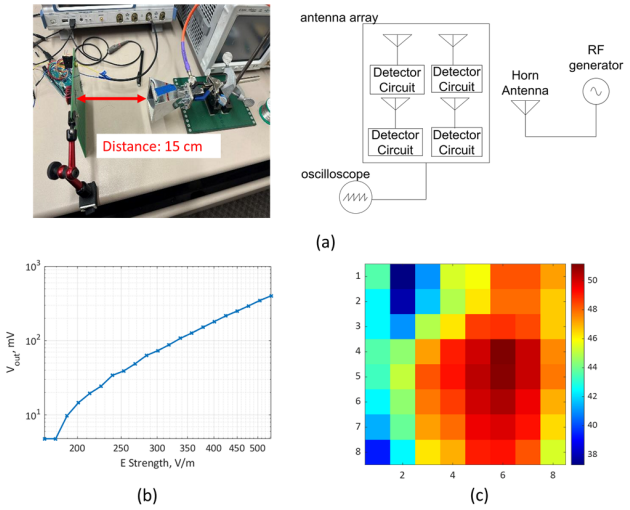

Fig. 8. Characterization of the proposed camera without an amplifier. (a) Measurement setup. (b) Sensitivity of the array at 11.25 GHz. (c) Example image produced by the sensor.

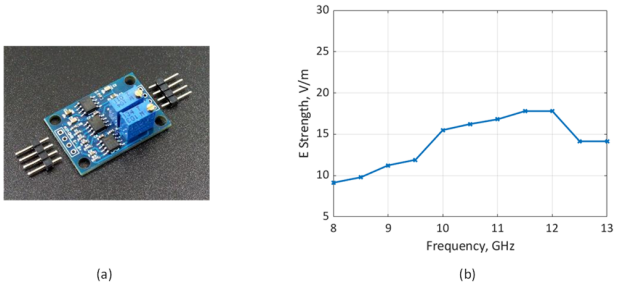

Fig. 9. Characterization of proposed camera with amplifier. (a) The amplifier AD 620. (b) Minimum detectable E field strength of the array with amplifier.

where $P_{antenna}$ is the antenna input power, G_{horn} is gain of the horn antenna, and d is, the distance between the antennas. The output voltage vs. the E-field strength is plotted in Fig. 7 (b). The minimum detectable E-field strength is about 30 V/m corresponding to the 0.1 mV detector output. Similarly, the frequency response of the combined circuit is measured, as shown in Fig. 7 (c). The E-field strength is fixed on 75 V/m, and the frequency is swept from 8 GHz to 12 GHz. The maximum output voltage is observed at 11.25 GHz and a second peak is located at 10 GHz. The system bandwidth is determined by the cut-off frequency of the antenna and the maximum operational frequency of the diodes and is approximately equal to 8-12 GHz.

B. Real-time Camera Sensor Characterization

The proposed 8 x 8 array sensor is characterized using the setup as shown in Fig. 8. The sensitivity and the image quality are evaluated. In this case, the output voltage of each element is measured by the 10-bit ADC of the Arduino board. The output signals or all elements are read by the serial interface and plotted in MATLAB. As shown in Fig. 8 (b), the minimum detectable voltage is about 4.9 mV, which is determined by the sensitivity of the on-board ADC (this voltage corresponds to the E-field strength of about 180 V/m). A typical image detected by the sensor directly illuminated by a horn antenna is shown in Fig. 8

Fig. 10. Periodic output signal of the sensor.

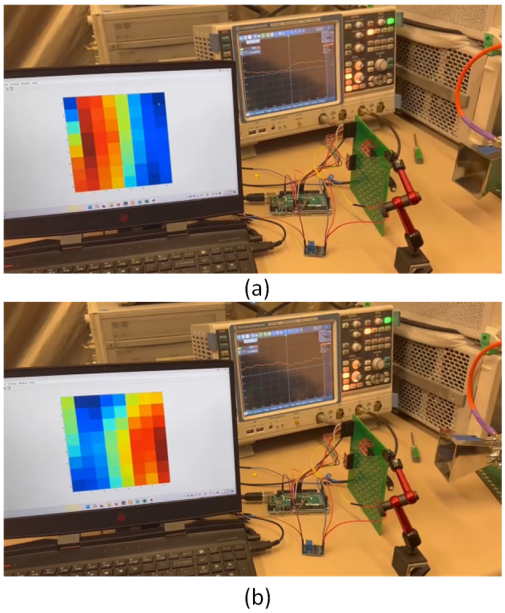

Fig. 11. Test example of the proposed camera. (a) The horn antenna points to the left. (b) The horn antenna points to the right.

(c). The value of the color axis is the output voltage of the array expressed in dBmV.

To increase the sensitivity of the camera, an instrumentation amplifier board (AD 620 [11]) shown in Fig. 9 (a) was added to the system. With the amplifier, the minimum detectable E field is decreased to 10-18 V/m in the frequency range from 8 to 12 GHz, as shown in Fig. 9 (b).

The frame rate of the camera is also measured. The signal at the output of the amplifier has a period of about 84 ms (Fig. 10), which corresponds to 12 frames per second.

To test and evaluate the performance of the real time camera, we let the image keep refreshing, while rotating the direction of the antenna quickly. The position of the hot spot on the screen moves with the movement of the antenna. Although the video of the test cannot be presented in the paper, two examples are shown in Fig. 11 (a) and (b) where the source antenna points to the left and right sides of the array, respectively. The hot spot locations correspond to the direction to the antenna and moves simultaneously with it.

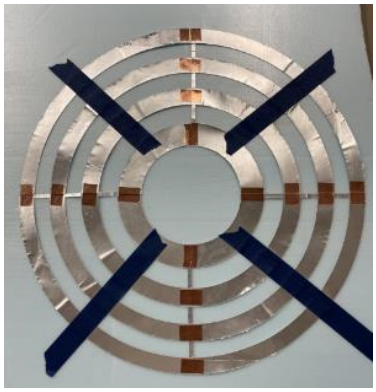

Fig. 12. Fresnel Zone Plate.

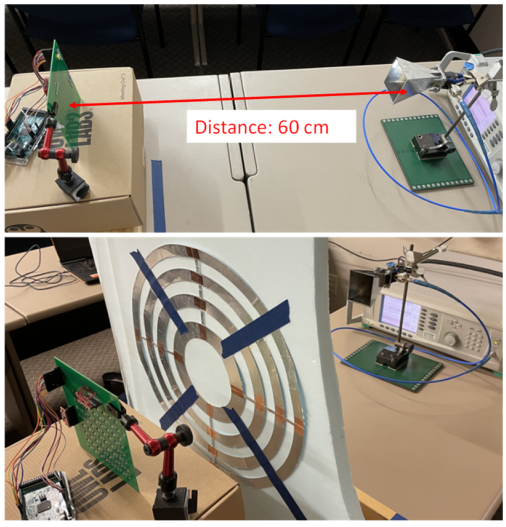

Fig. 13. Measurement setup for imaging. The distance between the antenna and the array is 60 cm. Image is recorded with and without the lens.

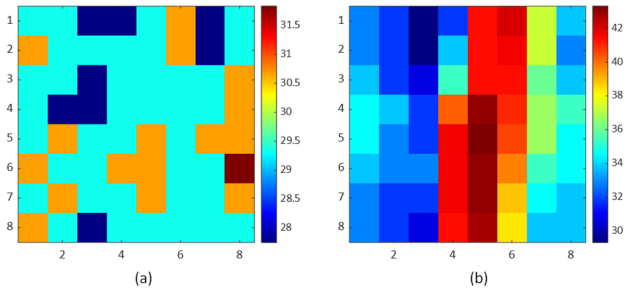

Fig. 14. Measurement results (Unit: dB mV). (a) Without the lens. (b) With the lens.

C. *Focusing and Imaging*

As the sensor outputs only the magnitude of the signals, the SAR (mathematical) focusing is not possible, and a separate focusing system is required. A physical lens or microwave holography [12] can be utilized for imaging. Here we chose to use a physical lens - the Fresnel zone plate, as shown in Fig. 12. The zone plate is designed to work at a frequency of 10 GHz and is made of aluminum foil. The radius for each layer for the half-wave zone is calculated by the equation [13]:

$$r_n = \sqrt{n\lambda F + \left(\frac{n\lambda}{2}\right)^2}, \qquad n = 1,2,3 \ldots \tag{3}$$

where λ is the operating wavelength, F is the focal length, and r_n are the radii of the layers. The focal length of the designed plate is 10 cm, and the aperture is 40 cm.

The imaging procedure is tested in the measurement setup as shown in Fig. 13. The antenna fed by an RF generator (at 20 dBm output power) is placed 60 cm away from the array. The location of the lens for imaging is given by the Gaussian lens formula:

$$\frac{1}{F} = \frac{1}{L_1} + \frac{1}{L_2} \tag{4}$$

where F, L_1, L_2 are the focal length, object distance and image distance respectively. For the 60 cm distance between the source and the sensor, the distance from the sensor to the lens is 13 cm. The output produced by the sensor is recorded with and without the lens.

The measurement results are shown in Fig. 14. In Fig. 14 (a) the output without the lens is produced. As the antenna is placed far away from the array (compared to the tests in sec. III A and B), the output of the sensor is mostly noise around the 30 dBmV mean value (at a 60 cm distance the field produced by the antenna is nearly uniform withing the aperture of the sensor and the image contains mostly the measurement noise). After adding the lens, the image of the antenna is focused on the array plane, as shown in Fig. 14 (b). A clear 41 dBmV spot in the middle of the sensor corresponding to the source antenna placed at the axis of the imaging system can be seen.

IV. Conclusion

In the paper, we proposed a real-time microwave camera for the EMI source imaging. A prototype 8 x 8 array working in the X-band is designed and presented. Zero-bias diode detectors are utilized, and low frequency multiplexers are used for switching the detector outputs, thus reducing the complexity and cost of the array. The performance of the antenna, the detector circuit, and the array are characterized separately. The sensitivity of the array is estimated at a 10-18 V/m level. The frame rate of the array is about 12 Hz, which can be considered real-time. To focus and imaging radiation source, a Fresnel zone plate is proposed and designed. The measurement results demonstrate a successful imaging of a single point source.

The future work of the proposed real-time camera includes building a larger and practical array, mitigating the coupling between the adjacent elements, and applying the system to realistic DUTs for EMI source imaging.

Acknowledgment

This paper is based upon work supported partially by the National Science Foundation under Grant No. IIP-1916535.

References

[1] P. Maheshwari, V. Khilkevich, D. Pommerenke, H. Kajbaf and J. Min, "Application of emission source microscopy technique to EMI source localization above 5 GHz," *2014 IEEE International Symposium on Electromagnetic Compatibility (EMC)*, 2014, pp. 7-11.

[2] P. Maheshwari, H. Kajbaf, V. V. Khilkevich and D. Pommerenke, "Emission Source Microscopy Technique for EMI Source Localization," in *IEEE Transactions on Electromagnetic Compatibility*, vol. 58, no. 3, pp. 729-737.

[3] L. Zhang et al., "Sparse Emission Source Microscopy for Rapid Emission Source Imaging," in *IEEE Transactions on Electromagnetic Compatibility*, vol. 59, no. 2, pp. 729-738, April 2017.

[4] J. Li, J. Zhou, S. Yong, Y. Liu and V. Khilkevich, "Automatic sparse ESM scan using Gaussian process regression," *2020 IEEE International Symposium on Electromagnetic Compatibility & Signal/Power Integrity (EMCSI)*, 2020, pp. 671-675.

[5] M. Sørensen, H. Kajbaf, V. V. Khilkevich, L. Zhang and D. Pommerenke, "Analysis of the Effect on Image Quality of Different Scanning Point Selection Methods in Sparse ESM," in *IEEE Transactions on Electromagnetic Compatibility*, vol. 61, no. 6, pp. 1823-1831, Dec. 2019.

[6] Xiaorui Liu, Xian Li, Hang Su, Yuefang Zhao, Shuzhi Sam Ge,"The Opening Workspace Control Strategy of a Novel Manipulator-driven Emission Source Microscopy System", *ISA Transactions*, 2022.

[7] Y. Liu, J. Li, C. Hwang and V. Khilkevich, "Near-Field Scan of Multiple Noncorrelated Sources Using Blind Source Separation," in *IEEE Transactions on Electromagnetic Compatibility*, vol. 62, no. 4, pp. 1376-1385, Aug. 2020.

[8] M. T. Ghasr, M. A. Abou-Khousa, S. Kharkovsky, R. Zoughi and D. Pommerenke, "Portable Real-Time Microwave Camera at 24 GHz," in *IEEE Transactions on Antennas and Propagation,* vol. 60, no. 2, pp. 1114-1125, Feb. 2012.

[9] *BAT15-04W Series silicon RF Schottky diode pair*, Infineon, Oct. 2018. [Online]. Available: https://www.infineon.com/dgdl/Infineon-BAT15-04W-DS-v01_00-EN.pdf?fileId=5546d46265f064ff016638961e2b4e86

[10] *Field Strength Calculation*, A.H. Systems. [Online]. Availble: https://www.ahsystems.com/EMC-formulas-equations/field-intensity-calculation.php

[11] *Low Cost Low Power Instrumentation Amplifier AD620*, Analog Devices. [Online]. Available: https://www.analog.com/media/en/technical-documentation/data-sheets/AD620.pdf

[12] G. Tricoles and N. H. Farhat, "Microwave holography: Applications and techniques," in *Proceedings of the IEEE*, vol. 65, no. 1, pp. 108-121, Jan. 1977.

[13] P. -L. Chi, C. -H. Pao, M. -H. Huang and T. Yang, "High-Gain Patch-Fed 3D-Printing Fresnel Zone Plate Lens Antenna for 60-GHz Communications," *2018 IEEE International Symposium on Antennas and Propagation & USNC/URSI National Radio Science Meeting*, 2018, pp. 597-598.